Peak splitting and locking behavior arising from Fano interference between localized surface plasmons and cavity modes

Penggang Li,[1,*] Li Ji,[2,*] Na Gao,[1] He Wang,[1] Shucheng Ge,[1] Kai Huang,[1,†] Junyong Kang,[1,‡] and Edward T. Yu[2]

[1]*Collaborative Innovation Center for Optoelectronic Semiconductors and Efficient Devices, Department of Physics, Xiamen University, Xiamen 361005, People's Republic of China*

[2]*Department of Electrical and Computer Engineering, Microelectronic Research Center, The University of Texas at Austin, Austin, Texas 78758, USA*

(Received 27 March 2016; revised manuscript received 29 May 2018; published 14 March 2019)

Coupling localized surface plasmons (LSPs) in Au nanostructure arrays to Fabry-Pérot cavity modes, both peak splitting and peak locking behaviors can be observed when light is incident normally into the cavity from different directions. These phenomena can be quantitatively described by a model based on modified Fresnel equations, and thus be interpreted as an extended Fano resonance effect. Both the peak splitting and peak locking behaviors arise from the interference between localized surface plasmon resonance and cavity modes with different initial phase difference. When the phase difference of the cavity state and the LSP state is π or 0, the superposition between a cavity resonance mode and a localized surface plasmon mode can result in the peak splitting or peak locking. Experimental results demonstrate that the separation energy between the split peaks changes with the volumes and densities of the Au nanoparticles and agree with the numerical calculation results quite well.

DOI: 10.1103/PhysRevB.99.125420

In 1961, when studying the autoionizing states of atoms, Fano discovered a new type of resonance, Fano resonance, arising from the constructive and destructive interference of a narrow discrete (Lorentzian) resonance with a broad spectral line or continuum [1]. Since then, Fano resonance have been found in various systems, such as quantum dots, nanowires, tunnel junctions, prism-coupled micropillars, and photonic crystals [2–6]. Especially within the past decade, Fano resonance in plasmonic nanostructures, such as diffraction gratings and hole/particle arrays, has been observed and extensively studied [7–10]. Localized surface plasmon resonances (LSPRs) originate from the collective oscillation of free electrons that are confined within the metal nanoparticle when coupled with the light [11–13]. The particle polarizability has a Lorentzian form [14]. Thus when interference occurs between one LSPR mode and another Lorentzian spectral line or continuum, Fano resonance may occur also (such as the coupling between the dipole mode and the quadrupole or octupole modes of LSP resonances [15,16], and coupling between the continuum Fresnel reflection, respectively [17,18]).

Many light generations involve transitions between the electronic energy levels of a quantum system. It has been revealed that if the interaction between the emitter and its local optical environment is sufficiently strong, then the energy levels, corresponding to the emissions, can be altered and be inextricably linked with the levels (modes) of the local optical environment, which is the so-called strong coupling [19,20]. If the coupling is very weak, compared to other relevant energy scales, the modification of the original energies levels, due to the coupling effect, is negligible, which is the weak-coupling regime. Strong coupling between light and matter has been studied extensively by combining optical cavities and materials that support dipole excitations [21,22], most of which investigate the strong-coupling regime by observing anticrossing dispersions from the emission, transmission, or reflectance spectra. During the past decades, it has been revealed that when ordered metallic nanoparticle (NP) arrays interact with Fabry-Pérot (FP) cavities, the LSP resonance modes show anticrossing mode splitting behaviors with the waveguide modes as well [23,24]. Those mode splitting behaviors are usually regarded as the strong-coupling effect and the dispersion diagrams are usually described by solving the Hamiltonian eigenvalue equations [24–26].

By solving the Hamiltonian eigenvalue equations with mode dampings, when the LSP resonance mode is coupled with an optical cavity mode, the observed peak splitting frequencies can be expressed as $\Delta E = 2\sqrt{g^2 - (\gamma_{LSP} - \gamma_{CAV})^2/16}$ [27,28], where g is the coupling strength between the LSPs and the cavity, γ_{LSP} is the damping of the LSPs, and γ_{CAV} is the damping of the cavity. Thus, considering the overlap between two Lorentzian (or Gaussian) distributions, the actual splitting could be visible only if the splitting energy ΔE is larger than the widths of the split modes $(\gamma_{LSP} + \gamma_{CAV})/2$ [19,29].

Here we investigate the coupling behaviors between the LSP resonance modes and FP cavity modes by positioning metallic NP arrays between a dielectric cavity with higher refractive index and a substrate with lower refractive index [Fig. 1(a)]. The high-reflection (HR) peaks show characteristic anticrossing peak splitting dispersion near the LSP

*These authors contributed equally to this work and should be considered co-first authors.

†k_huang@xmu.edu.cn

‡jykang@xmu.edu.cn

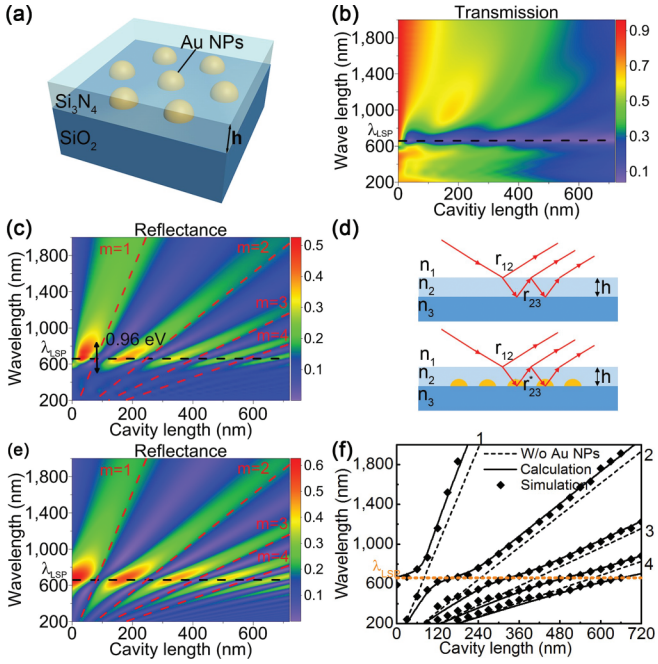

FIG. 1. Peak splitting behavior of LSP coupled optical cavity. (a) Schematic of the FP cavities on substrate with Au NP arrays for FDTD simulation. (b),(c) FDTD simulated transmittance and reflectance dispersions vs cavity thickness, respectively; the black dashed line indicates the LSP resonance wavelength and the red dashed lines indicate HR peak dispersions of the unperturbed FP cavity with particular m value. (d) Schematics of the FP cavities on substrates with/without Au NPs, respectively, showing partial wave decompositions when light is incident normally from the air to the cavity. (e) Calculated reflectance dispersion diagram of LSP coupled FP cavity by inserting Eq. (2) into (1). (f) HR peak dispersions extracted from the simulated and calculated data. Solid and dashed lines represent the HR peak dispersions of cavity with/without LSPs, respectively. The solid rectangular dots represent the simulated data extracted from the fringe maxima in (c).

resonance wavelength when light is incident normally from the air to the cavity, which is similar to the anticrossing dispersion in the strong-coupling regime [28,30,31]. However, the abovementioned requirement $\Delta E > (\gamma_{\mathrm{LSP}} + \gamma_{\mathrm{CAV}})/2$ is not satisfied. This indicates that the observed anticrossing dispersion in this system does not arise from the strong-coupling effect. However, when light is incident normally from the substrate to the cavity, a peak of the LSP mode remained unaltered or "locked" in the entire dispersion diagram, which is similar to the dispersion in the weak-coupling regime. Instead of using Hamiltonian eigenvalue equations, theoretical analysis shows that the observed peak splitting/peak locking behaviors can arise from the Fano interference between localized surface plasmons and cavity resonance modes. By superposition of a Lorentzian discrete state with a cavity resonance state with different initial phase difference, both "strong-coupling regime dispersionlike" and "weak-coupling regime dispersionlike" dispersion will appear. Experiments are designed to prove the theoretical predictions by fabricating Au NP arrays via annealing Au films with different film thicknesses. All measured peaks are in good accord with the theoretical prediction. The separation energy of the HR peak 1 increases with the Au film thickness before the annealing process when light is incident normally from the air into the cavity.

To investigate the coupling behaviors between the LSP resonance modes and FP cavity modes, Au NP arrays positioned between a dielectric cavity and substrate are employed [Fig. 1(a)]. Figure 1(b) shows the finite-difference time-domain (FDTD) simulated transmission dispersion vs cavity thickness. Transmission minima at approximately 660 nm, corresponding to the LSP resonance wavelength, are observed in all spectra regardless of the thickness of the cavity. Figure 1(c) shows the reflectance dispersion vs cavity thickness when light is incident normally from air into the cavity. Both the HR peaks and antireflection (AR) valleys split to two, near the LSP resonance wavelength. Since the lower branch of the split HR peak 1 is associated with the high-reflection peak of the Au NP arrays on the substrate without a cavity [32], we focus on this peak splitting behavior via the HR peaks. The unperturbed FP cavity HR peaks split into two anticrossing peaks near the LSP resonance wavelength. The cavity mode order m is calculated by $(m - 1/2)\lambda = 2nh$, where n is the refractive index of the cavity and h is the cavity thickness. The corresponding splitting energy of the HR peaks ΔE is measured to 0.96 eV at the anticrossing point of HR peak 1. However, at the anticrossing point of HR peak 1, the damping $\gamma_{\mathrm{CAV}} = 1.95\,\mathrm{eV}$ can be obtained from the reflectance spectrum of the cavity without Au NPs. Obviously, the requirement $\Delta E > (\gamma_{\mathrm{LSP}} + \gamma_{\mathrm{CAV}})/2$ is not satisfied.

By using a model based on the modified Fresnel coefficients [32,33], the observed peak splitting behavior can be quantitatively illustrated. According to the Fresnel equations, when light is incident normally from air ($n_1 = 1$) into a dielectric layer with thickness h and refractive index $n_2 = 2 + 0.05i$ deposited on substrate with refractive index $n_3 = 1.5$, the reflection coefficient r and the total reflectivity R can be written as

$$r = \frac{r_{12} + r_{23}e^{2i\beta}}{1 + r_{12}r_{23}e^{2i\beta}} \quad \text{and} \quad R = |r|^2, \tag{1}$$

where $r_{mn} = (n_m - n_n)/(n_m + n_n)$, $\beta = (2\pi/\lambda)n_2 h$. For a common dielectric interface [upper panel in Fig. 1(d)], the reflection coefficient r_{mn} is a real number, and the reflection phase change is either 0 or π. However, when there are metallic NP arrays located between substrate and dielectric cavity [lower panel in Fig. 1(d)], using the model based on modified Fresnel coefficients [17], the reflection coefficient r_{mn} should be modified as

$$r_{23}^{*} = \frac{n_2 - n_3 + i\frac{\omega}{c}\rho\alpha(\omega)}{n_2 + n_3 - i\frac{\omega}{c}\rho\alpha(\omega)}, \tag{2}$$

where $\alpha(\omega)$ is the frequency-dependent polarizability of a single NP and ρ is the surface density of NPs. If the interband transition of gold is not taken into consideration, it can be shown that the polarizability takes an essentially Lorentzian form [17,34]:

$$\alpha(\omega) \approx \frac{V\omega_p^2}{\omega_{\mathrm{LSPR}}^2 - \omega^2 - i\omega(\gamma_0 + F\omega^2)}, \tag{3}$$

where V is the volume of each metal NP, $\omega_p \approx 1.3 \times 10^{16}$ rad/s is the bulk plasma frequency of gold [17], and ω_{LSPR} is the resonance frequency of LSPs. The width of the resonance is determined by the resistive Drude damping factor $\gamma_0 \approx 2.5 \times 10^{13}$ rad/s and a factor $F = {\varepsilon_{\mathrm{eff}}}^{3/2}\omega_p^2 V/(9\pi c^3)$ that describes the radiative damping contribution due to the finite size of the particle, where $\varepsilon_{\mathrm{eff}}$ is an effective dielectric constant characterizing the surrounding medium.

Figure 1(e) shows the calculated reflectance dispersion diagram vs cavity thickness by inserting Eq. (2) into (1), where $\rho = 1 \times 10^{10}\ \mathrm{cm}^{-2}$, $V \approx 4.36 \times 10^4\ \mathrm{nm}^3$ are set as the simulation conditions, $\omega_{\mathrm{LSPR}} \approx 2.92 \times 10^{15}$ rad/s is obtained from the transmission spectra, and $\varepsilon_{\mathrm{eff}} = 3.24$ are obtained by unifying the wavelengths of the transmission valleys by using Au NP arrays in a homogeneous medium structure. The results show that the dispersion diagram is quite similar to that shown in Fig. 1(c). The separation energy is approximately 1.13 eV at the anticrossing point of peak 1, which is very close to that for the simulated dispersion.

Figure 1(f) shows the HR peaks extracted from the simulated and calculated dispersion. Simulated and calculated dispersion both show characteristic peak splitting behaviors, confirming the applicability of our model when explaining that the peak splitting occurred in an LSP coupled cavity. The deviation between the simulated and calculated data for a wavelength shorter than the LSP resonance wavelength can be attributed to the influence of the interband transition of gold, which is excluded in this model. The interband transition of gold can also explain the deviation between the simulated and calculated separation energies. At longer wavelength, the simulated and calculated data are in very good agreement. However, they are not asymptotic, but parallel to the unperturbed FP cavity modes without Au NPs. This can be attributed to the additional phase shifts at the interfaces between the cavities and the substrates at the long-wavelength region (see Fig. S1 inthe Supplemental Material [35]). When the cavity thickness is equals to 0, which means the Au NPs are located on the substrate without cavity, the simulated peak wavelength is shorter than the calculated peak wavelength. This is attributed a variation of the refractive index surrounding the Au NPs.

Figure 2(a) shows the FDTD simulated reflectance dispersion vs cavity thicknesses when light is incident normally from substrates into the cavity. The HR peaks are observed near the LSP resonance wavelength regardless of the thicknesses of the cavity, i.e., the HR peaks are locked at the LSP

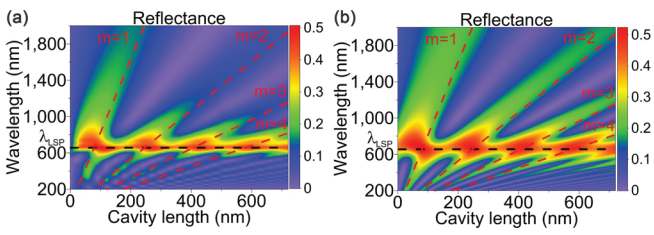

FIG. 2. Peak locking behavior of LSP coupled optical cavity. (a) FDTD simulated reflectance dispersion diagram of FP cavity with Au NPs located between the FP cavity and the substrates. (b) Calculated reflectance dispersion diagram of FP cavity with Au NPs by Eq. (4).

resonance wavelength. Usually, this phenomenon indicates the weak coupling for a dipole coupled cavity. Similar to the method we used above, this peak locking behavior can also be quantitatively explained using the modified Fresnel coefficients. For a common dielectric layer on a dielectric substrate, when the normal incident direction changes from air to the substrate, the reflectance coefficient can be obtained by simply replacing r_{12} by r_{32} and r_{23} by r_{21} in Eq. (1). However, when light is incident normally from substrate for the cavity/metal NPs/substrate structure, Eq. (1) is no longer suitable because of $r_{23}^* \neq r_{32}^*$ in Eq. (2). The reflectance coefficient should be modified to

$$r = r_{32}^* + \frac{t_{32}^* r_{21} t_{23}^* e^{2i\beta}}{1 - r_{21} r_{23}^* e^{2i\beta}}, \tag{4}$$

where $r_{32}^* = [n_3 - n_2 + i\frac{\omega}{c}\rho\alpha(\lambda)]/[n_3 + n_2 - i\frac{\omega}{c}\rho\alpha(\lambda)]$ and $t_{23}^* = \frac{n_2}{n_3} t_{32}^* = 2n_2/[n_3 + n_2 - i\frac{\omega}{c}\rho\alpha(\lambda)]$. For all parameters used for the numeric and the theory, the values of the indices are the same as that when light is incident normally from air into the cavity.

Figure 2(b) shows the calculated reflectance dispersion vs cavity thickness using Eq. (4). The peak locking dispersion is similar to that shown in Fig. 2(a).

Similar peak splitting and peak locking behaviors have been observed in some previous investigations related to the LSP coupled cavities [36,37]. Using our model, these behaviors can also be quantitatively illustrated (detail can be found in Fig. S2 in the Supplemental Material [35]).

It has been revealed that the modified Fresnel equation is a typical Fano function [17]. When the LSPs are placed on the surface of a dielectric medium, highly asymmetric Fano profiles can be observed in the reflectance spectra, arising from the constructive and destructive interference of a narrow discrete (LSP) resonance with a continuum (interface reflection). Thus the peak splitting and peak locking behaviors discussed above can be regarded as the extension of a Fano resonance by simply replacing the continuum with a cavity mode [1,2]. By superposing a Lorentzian LSP mode $a = \frac{i\gamma_{\mathrm{LSP}}}{2\varepsilon - i\gamma_{\mathrm{LSP}}}$ with a detuned cavity mode $b = \cos(\frac{\pi}{2\gamma_{\mathrm{CAV}}}\varepsilon - \Delta)$ with initial phase difference 0 or π as $|a \pm b|^2$ (see Figs. 3(a), 3(b), and Fig. S3 in the Supplemental Material [35] for derivation), both the peak splitting and peak locking dispersions can be illustrated (see Figs. 3(c), 3(d), and videos in the Supplemental Material [35]), where E_{LSP} is the LSP resonance energy, ε is a reduced energy defined by $E - E_{\mathrm{LSP}}$, and Δ represents a detuning between the LSP and cavity modes. $\gamma_{\mathrm{LSP}} = 0.2$ and $\gamma_{\mathrm{CAV}} = 1$ are the widths of the LSP mode and the cavity resonance mode, respectively. We can see that the peak splitting and peak locking behaviors can arise from the Fano interference between the LSP mode and the cavity mode. It is not necessary to shift the resonance frequencies due to the interaction between the LSP and cavity modes which the strong-coupling model needs.

All simulations were performed with commercial Lumerical FDTD SOLUTIONS (version 7.5) software. The schematic structures are shown in Fig. 1(a). In order to match the experimental condition, the refractive indices of the Si_3N_4 cavity and the quartz substrate are set as $2.0 + 0.05i$ and 1.5, respectively. The diameters and the densities of the

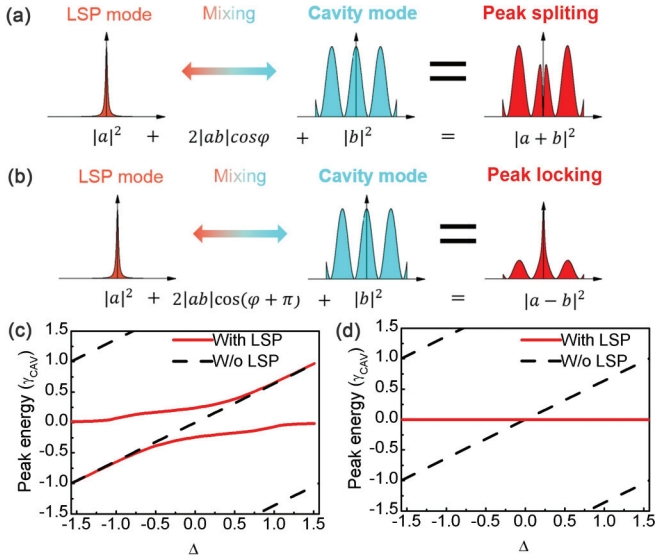

FIG. 3. Fano interference between the LSP modes and cavity modes. (a),(b) Schematics of peak splitting and locking behaviors arising from Fano interference, respectively. (c),(d) Peak splitting and locking dispersion diagrams when LSP modes are superposed with cavity modes with Δ ranging from $-\pi/2$ to $\pi/2$.

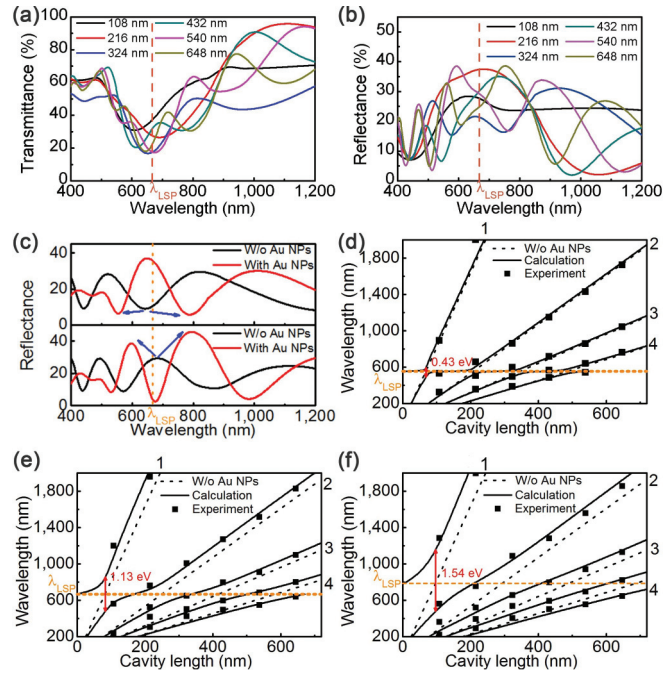

FIG. 4. Experimental results. (a),(b) Experimental transmission and reflectance spectra of the FP cavity with LSPs, respectively. (c) Experimental reflectance spectra with/without Au NP arrays when light is incident normally from the substrate into the cavity. The film thicknesses are approximately 324 (upper panel) and 432 nm (lower panel), respectively. The blue arrows are used to indicate that one peak (valley) was split into two. (d)–(f) HR peak dispersion diagrams extracted from the experimental and calculated data. The Au NP arrays were formed from 2, 5, and 8 nm Au films, respectively. Solid and dashed lines represent the HR peak dispersions of cavity with/without LSPs, respectively. The solid rectangular dots are extracted from the fringe maxima in the experimental reflectance spectra when light is incident normally from the air into the cavity.

semispherical Au NP arrays are set as 55 nm and 1.0×10^{10} cm^{-2}, respectively. The incident plane wave propagated perpendicular to the interface of two media from the z or $-z$ directions with the same incident energy density. The polarization direction of the incident wave is along the x direction. Au NPs were fabricated on quartz wafers. Au films with thickness of approximately 2, 5, and 8 nm were sputtered onto the substrates, followed by rapid thermal annealing in N_2 at 700 °C (for 2 nm Au films) or 800 °C (for 5 and 8 nm Au films) for 60 s to form Au NP arrays. Scanning electron microscopy (SEM) results show that the average diameters of the Au NP arrays are approximately 28, 55, and 248 nm, and the densities of the Au NP arrays are approximately 8.5×10^{10}, 1.0×10^{10}, and 2.2×10^{8}cm^{-2}, respectively. Then, Si_3N_4 films with different thicknesses were deposited to form the FP cavity by plasma-enhanced chemical vapor deposition (PECVD). The refractive index of the Si_3N_4 film at approximately 670 nm was measured to approximately $2.01 + 0.05i$ by an ellipsometer.

These as-prepared samples were characterized via transmittance and reflectance measurements. Figure 4(a) shows the measured transmittance spectra with different cavity thicknesses. The Au NP arrays between the cavities and the substrates are annealed from 5 nm Au films. Transmittance minima are presented around 667 nm in all samples, slightly larger than the simulated LSP resonance wavelength. Figure 4(b) shows the measured reflectance spectra when light is incident normally from the substrate into the cavity. Similar to that as shown in Fig. 2, HR peaks are shown close to the LSP resonance wavelength in all samples.

Figure 4(c) shows the typical measured reflectance spectra of samples with/without Au NPs when light is incident normally from the air into the cavity. The cavity thicknesses are approximately 324 and 432 nm, respectively. For the LSP coupled cavity, both HR and AR peaks split into two, when the unperturbed HR/AR peaks are close to the LSP resonance wavelength. Figure 4(d) shows the HR peak extracted from the experimental reflectance spectra (denoted as the solid rectangular dots) and the dispersion calculated by inserting Eq. (2) into (1) (denoted as the solid lines). Nearly all parameters are the same as those for calculating Figs. 1(e) and 1(f) except the experimental LSP resonance wavelength (667 nm). The measured spectra are in good accord with the calculated dispersion. The separation energy of peak 1 is approximately 1.13 eV as well. Furthermore, the separation energy can be tuned by changing the average volume and the density of the Au NPs. Figures 4(e) and 4(f) show the experimental and calculated HR peak dispersions when the Au NP arrays are annealed from 2 and 8 nm Au films, respectively. All experimental results are in good agreement with the calculated dispersions. The separation energies of HR peak 1 are approximately 0.43 and 1.54 eV, respectively.

In summary, we have demonstrated that when a FP cavity is coupled to LSPs, the HR peaks can split into two peaks and the peak dispersion shows anticrossing around the LSP resonance wavelength when light is incident normally from the cavity. The separation energy of the HR peak 1 is as large

as around 0.96 eV for gold NP arrays, with 55 nm in diameter in a density of 1.0×10^{10} cm^{-2}. Our study demonstrates that this peak splitting behavior can be quantitatively explained by simply modifying the interface reflection coefficient in the Fresnel equations. This method can also explain the peak locking behavior that occurs when light is incident normally from the substrate without applying any additional restricting conditions. Mathematically, we have elucidated that the peak splitting and peak locking behaviors can be deduced by the superposition between a cavity resonance peak and a Lorentzian form discrete LSP peak with different phase shifts. Thus, these behaviors can be regarded as an extended Fano resonance effect. The resonance frequencies shift due to the interaction between the LSP and FP mode of the cavity is not necessary. Furthermore, we also performed experiments in which all measured spectral data agree very well with the theoretical predictions. Transmission minima are shown in all samples close to the LSP resonance wavelength. When light is incident normally from the substrate, reflectance maxima are shown in all samples close to the LSP resonance wavelength. When light is incident normally from the air into the cavity, the HR peaks show characteristic peak splitting behaviors. The separation energy increases with increasing Au film thickness, which is used for Au NP formation via annealing.

We thank S. Y. Chen for helpful discussions and X. Yang for assistance. This work was supported by the National Key Research and Development Program (Grant No. 2016YFB0400903), the National Natural Science Foundation of China (Grants No U1405253, No. 61604124, No. 61874092, and No. 61874090), and the fundamental research funds for the Central Universities (Grants No. 20720160018 and No. 20720170098).

[1] U. Fano, Phys. Rev. **124**, 1866 (1961).
[2] A. E. Miroshnichenko, S. Flach, and Y. S. Kivshar, Rev. Mod. Phys. **82**, 2257 (2010).
[3] H. G. Luo, T. Xiang, X. Q. Wang, Z. B. Su, and L. Yu, Phys. Rev. Lett. **92**, 256602 (2004).
[4] A. C. Johnson, C. M. Marcus, M. P. Hanson, and A. C. Gossard, Phys. Rev. Lett. **93**, 106803 (2004).
[5] H. T. Lee and A. W. Poon, Opt. Lett. **29**, 5 (2004).
[6] M. V. Rybin, A. B. Khanikaev, M. Inoue, K. B. Samusev, M. J. Steel, G. Yushin, and M. F. Limonov, Phys. Rev. Lett. **103**, 023901 (2009).
[7] B. Luk'yanchuk, N. I. Zheludev, S. A. Maier, N. J. Halas, P. Nordlander, H. Giessen, and C. T. Chong, Nat. Mater. **9**, 707 (2010).
[8] F. Hao, Y. Sonnefraud, P. V. Dorpe, S. A. Maier, N. J. Halas, and P. Nordlander, Nano Lett. **8**, 3983 (2008).
[9] N. Verellen, Y. Sonnefraud, H. Sobhani, F. Hao, V. V. Moshchalkov, P. V. Dorpe, P. Nordlander, and S. A. Maier, Nano Lett. **9**, 1663 (2009).
[10] G. Bachelier, I. Russier-Antoine, E. Benichou, C. Jonin, N. Del Fatti, F. Vallee, and P. F. Brevet, Phys. Rev. Lett. **101**, 197401 (2008).
[11] U. Kreibig and M. Vollmer, *Optical Properties of Metal Clusters* (Springer, Berlin, 1995).
[12] E. Hutter and J. H. Fendler, Adv. Mater. **16**, 1685 (2004).
[13] S. Underwood and P. Mulvaney, Langmuir **10**, 3427 (1994).
[14] S. A. Maier, *Plasmonics: Fundamentals and Applications* (Springer, Berlin, 2007).
[15] C. F. Bohren and D. R. Huffman, *Absorption and Scattering of Light by Small Particles* (Wiley, New York, 1983).
[16] M. I. Tribelsky and B. S. Lykyanchuk, Phys. Rev. Lett. **97**, 263902 (2006).
[17] M. Svedendahl and M. Kall, ACS Nano **6**, 7533 (2012).
[18] M. Svedendahl, R. Verre, and M. Käll, Light: Sci. Applic. **3**, e220 (2014).
[19] P. Torma and W. L. Barnes, Rep. Prog. Phys. **78**, 013901 (2015).
[20] V. Savona, L. C. Andreani, P. Schwendimann, and A. Quattropani, Solid State Commun. **93**, 733 (1995).
[21] S. Groblacher, K. Hammerer, M. R. Vanner, and M. Aspelmeyer, Nature (London) **460**, 724 (2009).
[22] J. D. Teufel, D. Li, M. S. Allman, K. Cicak, A. J. Sirois, J. D. Whittaker, and R. W. Simmonds, Nature (London) **471**, 204 (2011).
[23] R. Ameling and H. Giessen, Nano Lett. **10**, 4394 (2010).
[24] A. Christ, S. G. Tikhodeev, N. A. Gippius, J. Kuhl, and H. Giessen, Phys. Rev. Lett. **91**, 183901 (2003).
[25] A. Delga, J. Feist, J. Bravo-Abad, and F. J. Garcia-Vidal, Phys. Rev. Lett. **112**, 253601 (2014).
[26] I. Rotter and J. P. Bird, Rep. Prog. Phys. **78**, 114001 (2015).
[27] T. Tawara, H. Gotoh, T. Akasaka, N. Kobayashi, and T. Saitoh, Phys. Rev. Lett. **92**, 256402 (2004).
[28] R. J. Thompson, G. Rempe, and H. J. Kimble, Phys. Rev. Lett. **68**, 1132 (1992).
[29] G. Khitrova, H. M. Gibbs, M. Kira, S. W. Koch, and A. Scherer, Nat. Phys. **2**, 81 (2006).
[30] T. K. Hakala, J. J. Toppari, A. Kuzyk, M. Pettersson, H. Tikkanen, H. Kunttu, and P. Torma, Phys. Rev. Lett. **103**, 053602 (2009).
[31] C. Weisbuch, M. Nishioka, A. Ishikawa, and Y. Arakawa, Phys. Rev. Lett. **69**, 3314 (1992).
[32] K. Huang, W. Pan, J. F. Zhu, J. C. Li, N. Gao, C. Liu, L. Ji, E. T. Yu, and J. Y. Kang, Sci. Rep. **5**, 18331 (2015).
[33] D. Bedeaux and J. Vlieger, *Optical Properties of Surfaces* (Imperial Collage Press, London, 2001).
[34] I. Zoric, M. Zach, B. Kasemo, and C. Langhammer, ACS Nano **5**, 2535 (2011).
[35] See Supplemental Material at http://link.aps.org/supplemental/10.1103/PhysRevB.99.125420 for additional results and supplemental video.
[36] R. Ameling and H. Giessen, Laser Photon. Rev. **7**, 141 (2013).
[37] M. Bahramipanah, S. Dutta-Gupta, B. Abasahl, and O. J. Martin, ACS Nano **9**, 7621 (2015).